



**Reversible open-close conformational switching of a nano-size metalloporphyrin dimers triggered by light and temperature**

Journal:	<i>Dalton Transactions</i>
Manuscript ID	DT-ART-01-2024-000223.R2
Article Type:	Paper
Date Submitted by the Author:	08-Mar-2024
Complete List of Authors:	Shah, Syed; Indian Institute of Technology Kanpur, Department of Chemistry Singh, Ajitesh ; Indian Institute of Technology Kanpur, Department of Chemistry Goswami, Debabrata; IIT Kanpur, Chemistry Ishida , Masatoshi ; Tokyo Metropolitan University Rath, Sankar; Indian Institute of Technology Kanpur, Department of Chemistry



## Reversible open-close conformational switching of a nano-size metalloporphyrin dimers triggered by light and temperature

Received 00th January 20xx,  
Accepted 00th January 20xx

DOI: 10.1039/x0xx00000x

Syed Jehanger Shah,<sup>a</sup> Ajitesh Singh,<sup>a</sup> Debabrata Goswami,<sup>a</sup> Masatoshi Ishida<sup>b</sup> and Sankar Prasad Rath<sup>\*a</sup>

The current work demonstrates the reversible control of substantial molecular motion in 'nano-sized' molecules, where two structural isomers can 'open' and 'close' their cavities using light or heat. The isomers differ widely in their photophysical properties, including colour, polarity, two-photon absorption and  $\pi$ -conjugation, and can easily be separated through column chromatography and thus have wide applicability.

### Introduction

Over the last few decades, the field of synthetic molecular machines has received a great deal of attention due to the significant impact these types of machinery can have on the design of artificial, dynamic systems controllable by external stimuli and various potential applications ranging from biomedical to smart materials.<sup>1-8</sup> On a functional level, two distinguishable states can undergo reversible interconversion by a back-and-forth type of motion using a variety of external stimuli to utilise their potential fully.<sup>1,2</sup> Azobenzenes, stilbenes, diarylethenes, spiropyrans, and hydrazones are prominent examples of such molecular switches.<sup>3-6</sup> Among these molecular switches, photochromic molecules are getting much attention due to reversible light-triggered switching, which is requisite for imaging nano structures.<sup>5-8</sup> The benefit of using light to regulate molecular mobility over chemical reactants is that it provides exceptional spatiotemporal control.

Herein, we demonstrate a novel and unique system controlling large molecular motion by external stimuli based on an 'open'-'close' reversible switching of 'nano-size' molecules. Besides their large structural changes, it is also interesting to note large differences in their optical, chemical and molecular properties, including colour, polarity, and  $\pi$ -conjugation through the bridge. Such distinct differences between the two structural isomers enable easier separation from the reaction mixture through column chromatography. The spatial orientation between the two porphyrin rings is known to control

inter-ring interactions, while the nature of the bridge dictates potential electronic communications between them.<sup>9-14</sup> Interestingly, the isomers that are demonstrated in the present investigation are reversibly interconvertible to each other by the application of light and temperature (Fig. 1). Their molecular structures have been determined by the single crystal X-ray diffraction studies and the facile 'open-close' transformation can easily be monitored visually by their colour changes and also spectroscopically using UV-vis-NIR, emission, two-photon absorption and <sup>1</sup>H NMR. Furthermore, extensive computational studies enable us to understand insights of such interconversion and their electronic nature.

### Results and discussion

Starting from 5-(2,6-dichlorophenyl)dipyrromethane-bridged porphyrin dimer (i.e., MDP<sup>13a</sup> in Scheme S1), both 'close-form' **1•M** and 'open-form' **2•M** (M = Cu, Ni) were obtained upon simple stirring with chemical oxidants such as 2,3-dichloro-5,6-dicyano-1,4-benzoquinone (DDQ) or *p*-chloranil. Interestingly, good synthetic yields of **1•M** and **2•M** were achieved only by stirring at different time intervals (Fig. S1). The formation of these complexes was supported by electrospray ionization (ESI) mass spectrometry, which displays intense molecular ion peaks with  $m/z = 1501.5819$  for [**1•Cu** + H]<sup>+</sup> and 1491.5654 for [**1•Ni** + H]<sup>+</sup>; the experimental isotopic distribution pattern matches exactly with the theoretical ones (Figs. S2-S3). Separately, **2•M** was synthesized by our reported method.<sup>13a</sup> Indeed, large structural changes between **1•M** and **2•M** bring disparity in their molecular properties like solubility, polarity, etc., which makes their separation easier *via* silica gel column chromatography. The 'close' form was found to be less polar than the 'open' form and was observed experimentally during separation through silica gel column chromatography. The polarity-dependent spectral changes are observed in various solvents and the results are shown in Fig. S4.

<sup>a</sup> Department of Chemistry, Indian Institute of Technology Kanpur, Kanpur 208016, India. E-mail: sprath@iitk.ac.in; Fax: +91-512-259-7436; Tel: +91-512-259-7251

<sup>b</sup> Department of Chemistry, Graduate School of Science, Tokyo Metropolitan University, Hachioji, Tokyo 192-0397, Japan.

<sup>c</sup> † Electronic Supplementary Information (ESI) available: Synthesis and characterization of all complexes. Instrumentation, experimental and computational details, spectroscopic characterization, and computational results. CCDC 2308953 contain the supplementary crystallographic data of **1•Cu**. For ESI and crystallographic data in CIF or other electronic format see DOI:Address here

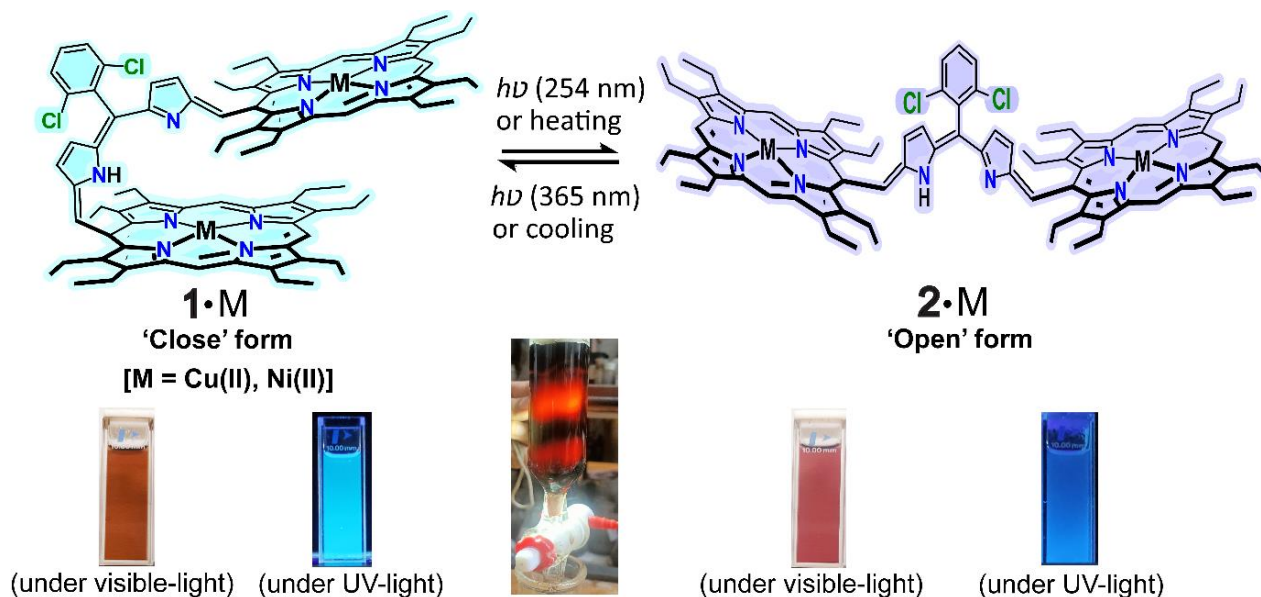


Fig. 1 Schematic representation of a reversible 'open-close' conformational switch. Colours of Cu(II) complexes in dichloromethane at 295K are shown.

Single crystals of **1•Cu** were grown via slow diffusion of n-hexane into the dichloromethane solution of the complex at room temperature in air at dark. The structure (Figs. 2, S5-S6, Table S1) was unambiguously elucidated by X-ray crystallographic analysis. The porphyrin planes are nearly cofacial to each other with a dihedral angle of 15.09° and the Cu•••Cu non-bonding distance is 7.41 Å. The average Cu–Np distance is 2.000(4) Å which falls within the range observed for the four-coordinate Cu(II)porphyrinates.<sup>13a,b</sup> **1•Cu** possesses a planar dipyrromethene bridge with significant alteration in the bond lengths and angles to make a  $\pi$ -conjugated 'close' structural scaffold which is also reflected in the appearance of an intense low-energy band in the UV–visible spectrum (*vide infra*). Porphyrin macrocycles also exhibited distortion; however, the distortion is less pronounced in **1•Cu** when compared to **2•Ni** (Table 1). Furthermore, the non-bonding Cu•••Cu distance of 7.41 Å in **1•Cu** is remarkably less as compared to the **2•Ni**<sup>13a</sup> in which Ni•••Ni distance is 16.39 Å. The substantial structural changes from **2•Ni** to **1•Cu** readily discernible in the crystal structures, while the conjugation through the bridge is reflected in the alternative bond distances of the bridging atoms (Table 1).<sup>13,14</sup>

Although both 'open' and 'close' complexes were synthesized separately but were seen to be isomerized under the application of light and temperature. Such conformational change was monitored *in situ* using various spectroscopic techniques such as UV-vis-NIR and <sup>1</sup>H NMR spectroscopies. The closed complex, **1•Ni**, displays a sharp Soret band at 400 nm, a Q-band at 563 nm, and an intense broad low-energy band in the NIR region centered at 866 nm. While the 'open' complex **2•Ni** has a red-shifted low-energy band at around 895 nm, distinguishing it from the 'close' complex. On heating **1•Ni**, a drastic change was observed in the UV-vis-NIR spectra with a red shift of the low-energy band from 866 to 895 nm to form **2•Ni**. When the same complex was cooled down, **1•Ni** was restored. The result showed complete reversible

conformational switching under thermal conditions as demonstrated in the appearance of clear isosbestic points in the electronic absorption spectra and was also seen between **1•Cu** and **2•Cu** (Figs. 3A and S7).

Similar 'open'-'close' conformational switching was also observed after light irradiation. At 365 nm UV-light, the 'open' complex switches to 'close' complex as observed after colour change from blue to bright sky-blue (Scheme 1). The change was also observed in the UV-vis-NIR spectra of **2•Ni** where a low-energy band at 895 nm gets blue-shifted to 866 nm along with slight broadness in the band at 563 nm to produce **1•Ni** (Fig. S8).

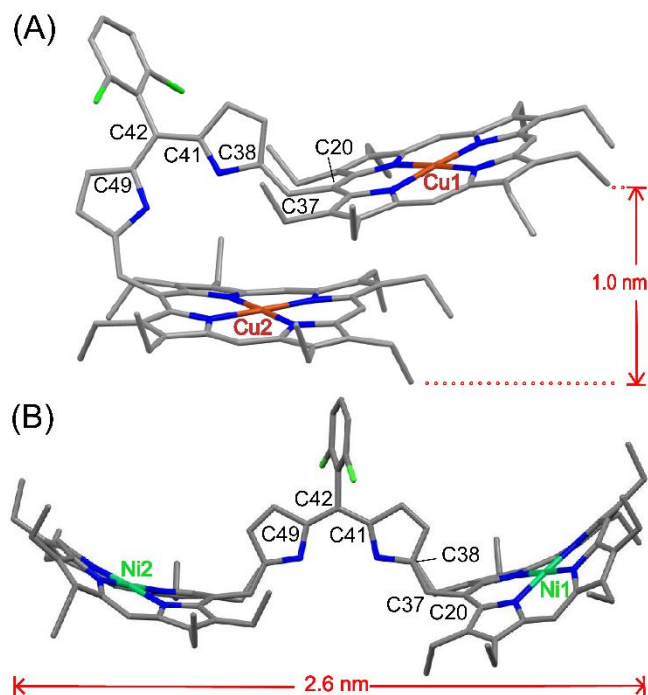
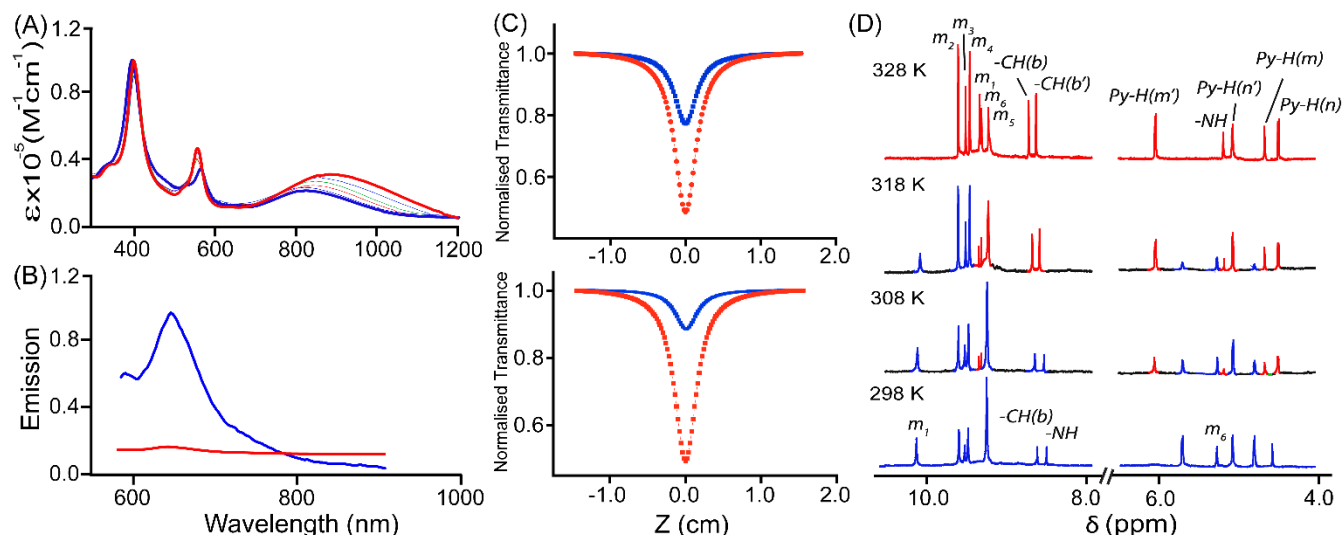


Fig. 2 Molecular structures (at 100 K) of (A) **1•Cu**, and (B) **2•Ni**<sup>13a</sup> (H atoms and solvent molecule, have been omitted for clarity).



**Fig 3.** (A) UV-vis-NIR (in  $\text{CH}_2\text{Cl}_2$ ) absorption spectra upon heating  $1\bullet\text{Ni}$  (blue line) to form  $2\bullet\text{Ni}$  (red line) and *vice-versa* on cooling with isosbestic points at 422, 528 and 700 nm. (B) Normalized emission spectra (in degassed  $\text{CH}_2\text{Cl}_2$  at 295 K) of  $1\bullet\text{Cu}$  (blue line) and  $2\bullet\text{Cu}$  (red line), excited at 560 nm. (C) Z-Scan signatures of  $1\bullet\text{Cu}$  (blue line),  $2\bullet\text{Cu}$  (red line) in the top and  $1\bullet\text{Ni}$  (blue line),  $2\bullet\text{Ni}$  (red line) in the bottom at maxima values of two-photon absorption at  $\lambda_{\text{ex}} = 800$  nm, and (D)  $^1\text{H}$  NMR (in  $\text{CDCl}_3$ ) spectral changes of  $1\bullet\text{Ni}$  (blue line) obtained upon increasing the temperature upto 328 K to form  $2\bullet\text{Ni}$ , proton numbering scheme is shown in Fig. S14 in SI.

**Table 1.** Selected structural parameters of the complexes.

Complex	$1\bullet\text{Cu}$	$2\bullet\text{Ni}^e$
M-N <sub>p</sub> (Å) <sup>a</sup>	2.000(4)	1.900(5)
$\Delta_{24}$ (Å) <sup>b</sup>	0.13	0.34
M...M(Å) <sup>c</sup>	7.41	16.39
$\theta$ (°) <sup>d</sup>	14.22	52.53
C20-C37(Å)	1.490(7)	1.474(8)
C37-C38(Å)	1.343(8)	1.331(9)
C41-C42(Å)	1.447(7)	1.399(9)
C42-C49(Å)	1.363(7)	1.388(8)
C20-C37-C38(°)	125.2(5)	121.0(6)
C41-C42-C49(°)	120.5(5)	126.2(6)

<sup>a</sup>Average value. <sup>b</sup>Average displacement of atoms from the least-squares plane of the  $\text{C}_{20}\text{N}_4$  porphyrinato core. <sup>c</sup>Non-bonding distance between two metal centers. <sup>d</sup>Angle between two least-squares planes of the  $\text{C}_{20}\text{N}_4$  porphyrinato cores. <sup>e</sup>Taken from reference 13a.

The transformation of  $1\bullet\text{Ni}$  to  $2\bullet\text{Ni}$  was observed through the irradiation of a UV-light at 254 nm. Similar spectral changes were observed between  $1\bullet\text{Cu}$  and  $2\bullet\text{Cu}$  (Fig. S9). However, the conversion from 'close' to 'open' was found more efficient under thermal conditions but the reverse process was quicker under UV-light at 365 nm. The UV-vis-NIR spectra of the conformers were also simulated by the TD-DFT calculations, which reproduce the major features of the experimental spectra (Figs. 4 and S10). The well-delocalized  $\pi$ -electron over the molecule of  $2\bullet\text{Ni}$  contributed to the emergence of a larger and redshifted band based on singlet natural transition orbital (NTO) analysis (Fig. S11). In contrast, the NTO transition from the singlet hole and particle for  $1\bullet\text{Ni}$  involves the partial CT nature. The low-energy band intensities that appeared in the NIR region for  $1\bullet\text{Ni}$  and  $2\bullet\text{Ni}$  are thus dependent on the conformation.

The most interesting feature of this conformational switch is the large change observed in their photophysical properties like colour, polarity, luminescence, etc. The emission is shown only by 'close' molecules, while the 'open' form is non-fluorescent in both Ni and Cu complexes (Fig. 3B). Although, both Cu(II) and Ni(II) complexes are known to quench fluorescence as observed in their 'open' forms, but upon conformational switching to the 'close' form, a weak emission band was obtained possibly due to structural rigidity in the closed form out of non-covalent interactions between two porphyrin rings (*vide infra*) or any other reasons unknown to us.<sup>15</sup> Moreover, the colour change is appreciable enough to distinguish between the 'close' and 'open' forms under UV-light irradiation (Figs. 1 and S12). Using Rhodamine 6G as a reference, two-photon absorption (TPA) properties of these complexes were also determined by the open aperture Z-scan method with  $\lambda_{\text{ex}} = 800$  nm (Figs. 3C and S13).

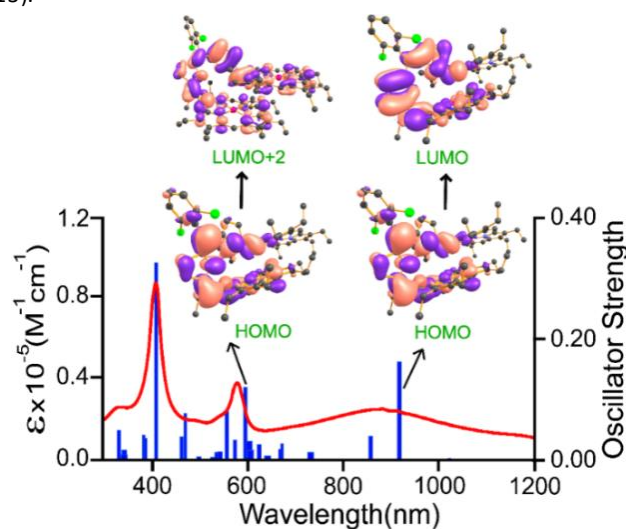


**Fig. 4.** Electronic absorption spectra (curved line, left axis) of  $1\bullet\text{Cu}$  in  $\text{CH}_2\text{Cl}_2$  and oscillator strengths (vertical line, right axis) obtained from TD-DFT calculations at the uB3LYP/6-31G\*\*/LANL2DZ level of theory, (the sigma value used in the spectra is 0.2 eV).

The TPA cross-sections ( $\sigma_2$ ) observed are:  $396 \pm 15$  GM for **1**•Cu,  $146 \pm 8$  GM for **1**•Ni,  $1390 \pm 66$  GM for **2**•Ni and  $1486 \pm 55$  GM for **2**•Cu. The increase in the TPA cross sections of 'open' complexes as compared to 'closed' ones can be attributed to the extended  $\pi$ -conjugation of the former (*vide infra*), which is reflected in their UV-vis-NIR spectra and DFT studies (*vide infra*) (Fig. 3C).<sup>16</sup>

The reversible conformational switch between **1**•Ni and **2**•Ni can easily be visualized using variable-temperature <sup>1</sup>H NMR spectroscopy (Fig. 3D; proton numbering scheme is shown in Fig. S14 and full spectra in Fig. S15). In **1**•Ni at 298K, the porphyrin rings are inequivalent, which leads to six meso signals centered at  $\delta = 10.13, 9.59, 9.51, 9.46, 9.25$  and  $5.31$  ppm, one of the meso signal as  $m_6$  is highly upfield shifted along with one of the bridging proton as expected<sup>17</sup> due to ring current effect. However, upon increasing temperature, the spectral pattern gradually changes due to the formation of **2**•Ni at higher temperature. During the process, the meso signal at 10.13 and at 5.31 ppm completely disappeared along with the formation of two new peaks at 9.30 and 9.33 ppm. Moreover, there are four signals for the bridging  $\beta$ -pyrrolic protons at 5.52, 5.11, 4.86, and 4.51 ppm and a relatively broad signal for the bridging-NH at 8.57 ppm for the 'close' form. These protons are also shifted at 328 K due to conformational change and are observed at 6.05, 5.07, 4.81, 4.47 (b-Hs), and 5.19 (NH) ppm in the 'open' form. Furthermore, the observed chemical shifts are also in good agreement with the calculated <sup>1</sup>H NMR spectrum of the complex (Fig. S16) by DFT GIAO method using the optimized structure (*vide infra*).

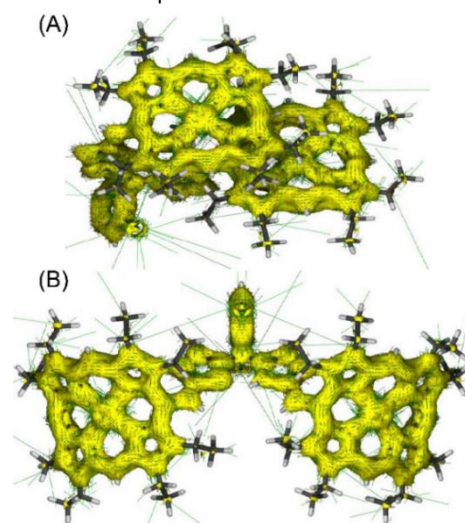
From the temperature dependent <sup>1</sup>H NMR spectral data during the conversion between **1**•Ni and **2**•Ni, the thermodynamic parameters were obtained using van't Hoff equation<sup>18</sup> (shown below) in which  $K_{eq}$  is the equilibrium constant;  $R$  is the gas constant in  $\text{cal K}^{-1} \text{mol}^{-1}$ ;  $\Delta H$  and  $\Delta S$  are the thermodynamic parameters *viz* change in enthalpy and entropy, respectively, and  $T$  is the temperature in Kelvin.

$$\ln(K_{eq}) = -\Delta H / RT + \Delta S/R$$

The  $\Delta H$  and  $\Delta S$  obtained from the plot for the conversion of 'close' to 'open' form in the nickel complex were  $5.38 \text{ kcal mol}^{-1}$  and  $15.53 \text{ cal K}^{-1} \text{mol}^{-1}$ , respectively (Fig. S17) which are also in good agreements with the results obtained in the DFT calculations (*vide infra*). The thermodynamic parameters also suggest that 'close' to 'open' conversion is an endothermic process as observed in the experiment.

The 'close' form was found to be less polar than the 'open' form and was observed experimentally during separation through column chromatography. As determined by DFT calculations, the geometry and structural parameters of **1**•M and **2**•M (M = Cu, Ni) (Figs. S18-S19) agreed well with the experimental data. The distinct difference in the molecular geometry is reflected in the larger dipole moment of 1.24 D obtained in the 'open' form compared to the 'close' form (0.58

D). This observation correlates well with the greater polarity of the 'open' form. The 'open' form was observed to have better



conjugation than 'close' form. This difference is reflected in the Fig. 5. AICD Plots for (A) **1**•Ni and (B) **2**•Ni with isocontour value of 0.05.

calculated HOMO–LUMO energy gaps with the orders being **1**•M > **2**•M (M = Cu, Ni) (Figs. 6A and S20-S21), which is consistent with the red-shift of the low-energy NIR band in **2**•M compared to **1**•M (Figs. 4 and S11). Also, **1**•Ni and **2**•Ni exhibit distinct Hückel aromaticity based on the nuclear-independent chemical shift (NICS) values and anisotropy of induced current density (AICD)<sup>19</sup> plots (Figs. 5 and S22-S25). Compared to **2**•Ni, the relatively larger extent of the aromatic character of **1**•Ni is presumably due to the localized  $\pi$ -electron over the restricted conjugation scaffold (*vide supra*).

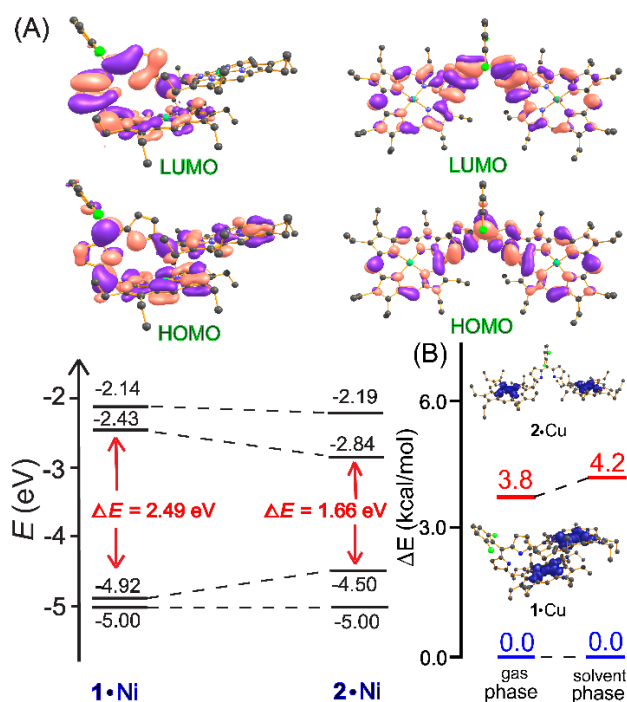
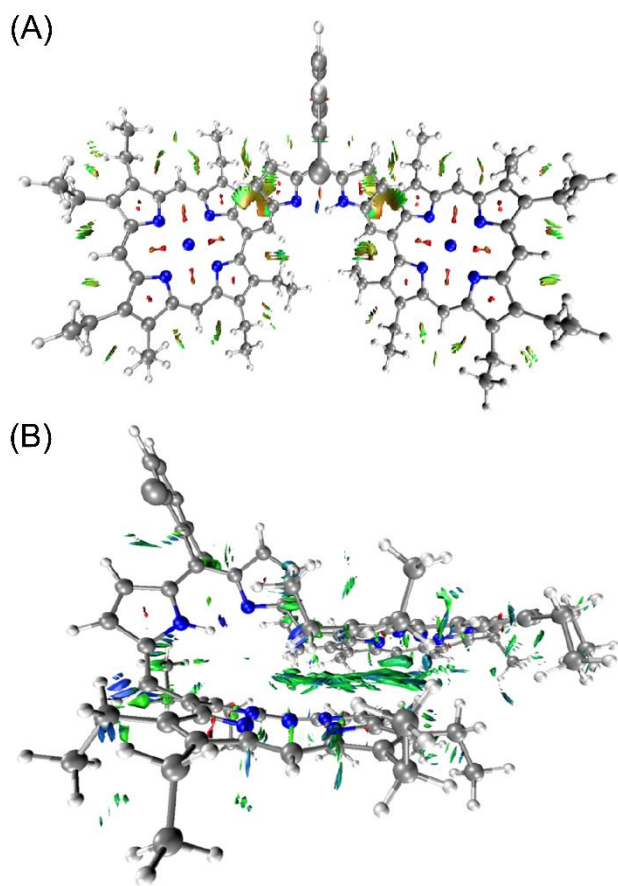


Fig. 6. (A) Energy diagrams and Kohn-Sham orbital representations of the HOMOs-LUMOs of **1**•Ni and **2**•Ni (isovalue = 0.015). (B) Relative energies of **1**•Cu (bottom) and **2**•Cu (top) in gas and solvent phases.

**2•Cu** (top) as calculated using CAM-B3LYP functional in DFT. Energies are relative to **1•Cu** and the spin density are shown.

Notably, the closed **1•Cu** is more stable than the open **2•Cu** by 3.8 and 4.2 kcal/mol in the gas and solvent phases, respectively (Fig. 6B). Likewise, the similar trend was observed in the nickel complexes (Fig. S26). However, the energy differences between the two forms are relatively small considering computational uncertainty, suggesting the potential for reversible switching under external perturbation as experimentally observed here. The greater thermodynamic stability of **1•M** is most likely due to the non-covalent interaction between two aromatic porphyrin macrocycles as evident from non-covalent interaction (NCI) plots (Figs. 7 and S27).



**Fig. 7.** NCI plots (isosurface value 0.05) of (A) **2•Cu**; front view and (B) **1•Cu**; side view green isosurface shows regions having noncovalent (van der Waals) interactions. Blue and red isosurfaces show regions having attractive and repulsive interactions, respectively.

The present conformational switching of the open-close molecular system seems to occur via  $Z \rightarrow E$  type geometrical transformation over the diastereomeric C=C bond connecting dipyrromethene (DPM) bridge and the porphyrin macrocycles. The 'close' form displays  $Z-E$  type correspondence, while the 'open' form appears to have  $E-E$  type (Fig. S28). Such a geometrical change between the 'close' and 'open' forms in the presence of UV-light is believed to occur via a radical mechanism as demonstrated earlier.<sup>5,20</sup> However, thermal

isomerization, like in azobenzene and stilbene, has also been observed between these  $E-Z$  and  $E-E$  type conjugated systems reported here. As previously suggested for the highly conjugated system,<sup>3,20,21</sup> the double bond character might be decreased due to extensive  $\pi$ -conjugation of the system that leads to a dramatic fall in the energetic barrier for rotation, which is otherwise very high.

## Conclusions

In summary, two structural isomers of 'nano-size' molecules have been demonstrated here that reversibly 'open' and 'close' their cavities triggered by light and temperature which can be monitored by using UV-vis-NIR, emission, and <sup>1</sup>H NMR spectroscopies. The isomers differ largely in their structure and photophysical properties enabling easier separation through column chromatography and thus have wide practical applicability.

## Experimental Section

### Materials

All the reagents and solvents were purchased from commercial sources and purified by standard procedures before use. Metal complexes, MDP (M= Ni, Cu), and **2•M** were prepared according to the literature procedures.<sup>13a</sup> The preparations of **1•Ni** and **1•Cu**, reported in the present work, are described below.

### Syntheses

**Synthesis of 1•Ni:** To a solution of MDP (50 mg, 0.033 mmol) in CH<sub>2</sub>Cl<sub>2</sub> (100 mL), DDQ (15 mg, 0.066 mmol) dissolved in acetonitrile was added, and the reaction mixture was stirred at room temperature for 30 min. The reaction mixture was then evaporated to complete dryness and further redissolved in CH<sub>2</sub>Cl<sub>2</sub> (100 mL) and washed initially with an aqueous solution of NaHCO<sub>3</sub> (2 × 200 mL), and then with water (3 × 200 mL). The combined solution was then evaporated to complete dryness, and it was further subjected to silica gel column chromatography (CH<sub>3</sub>OH/CH<sub>2</sub>Cl<sub>2</sub> 1:99 v/v) to yield the desired product as a light brownish solid. Yield: 39 mg (78%). <sup>1</sup>H NMR (CDCl<sub>3</sub>, 295 K, ppm): 10.13 (s, 1H; *meso-H*), 9.59 (s, 1H; *meso-H*), 9.51 (s, 1H; *meso-H*), 9.46 (s, 1H; *meso-H*), 9.25 (s, 2H; *meso-H*), 8.65 (s, 1H; *CH(b)*), 8.57 (s, 1H; *NH*), 7.10 (d, 2H; *Ph-H*), 6.95 (t, 1H; *Ph-H*), 6.05 (d, 1H; *Py-H*), 5.19 (s, 1H; *meso-H*), 5.07 (d, 1H; *Py-H*), 4.81 (d, 1H; *Py-H*), 4.47 (d, 1H; *Py-H*), 4.02-3.65 (m, 36H; -CH<sub>2</sub>(por) and (s, 1H; *CH(b')*), 2.23-0.89 (m, 54H; -CH<sub>3</sub>(por)). UV-vis-NIR (CH<sub>2</sub>Cl<sub>2</sub>) [ $\lambda_{max}$ , nm ( $\epsilon$ , M<sup>-1</sup> cm<sup>-1</sup>)]: 400 (1.0 × 10<sup>5</sup>), 563 (4.1 × 10<sup>4</sup>), 866 (2.8 × 10<sup>4</sup>).

**Synthesis of 1•Cu:** Yield: 42 mg (84%). UV-vis-NIR (CH<sub>2</sub>Cl<sub>2</sub>, 295 K) [ $\lambda_{max}$ , nm ( $\epsilon$ , M<sup>-1</sup> cm<sup>-1</sup>)]: 401 (1.0 × 10<sup>5</sup>), 560 (5.5 × 10<sup>4</sup>), 846 (3.1 × 10<sup>4</sup>).

### Instrumentation

UV-vis-NIR measurements were performed on the Perkin Elmer spectrometer and on the Agilent Cary 8454 UV-vis spectrometer. Emission spectra were recorded on the Agilent-Carey Eclipse spectrometer.  $^1\text{H}$  NMR spectra were recorded on a JEOL 500 MHz instrument. The residual  $^1\text{H}$  resonances of the solvents were used as a secondary reference.

### X-ray Structure Solution and Refinement

Crystals were coated with light hydrocarbon oil and mounted in the 100 K dinitrogen stream of a Bruker SMART APEX CCD diffractometer equipped with CRYO industries low-temperature apparatus, and intensity data were collected using graphite-monochromated  $\text{MoK}\alpha$  radiation ( $\lambda=0.71073\text{\AA}$ ). The data integration and reduction were processed with SAINT software.<sup>22</sup> An absorption correction was applied.<sup>23</sup> Structures were solved by the direct method using SHELXS-97 and were refined on  $F^2$  by full-matrix least-squares technique using the SHELXL-2018 program package.<sup>24</sup> Non-hydrogen atoms were refined anisotropically. The hydrogen atoms were included in geometrically calculated positions in the refinement and were refined according to the "riding model". The complex contains one severely disordered dichloromethane solvent molecule which could not be modelled properly due to weakly diffracting nature of the crystals and thus, the SQUEEZE routine of PLATON<sup>25</sup> was used to remove such unbound and highly disordered solvent molecule. Diagram showing the residual density plot of the X-ray structure of  $1\cdot\text{Cu}$  is shown in Fig. S29.

### Two-photon absorption measurement

To measure the two-photon absorption cross-section (TPACS)<sup>26</sup>  $\sigma_2$ , we have used an open aperture Z-Scan technique with a 1kHz Ti:Sapphire amplified laser (Coherent Astrella) beam centred at 800 nm with a pulse width of 35 fs. The laser beam is focused using a 10 cm lens; samples were placed in a 1 mm cuvette and scanned across the focus on a motorized translation stage with a spatial resolution of 0.1  $\mu\text{m}$ . The beam transmitted through the sample is collected and collimated using another lens and then focussed onto the detector using another lens. The change in the intensity of the light that falls on the detector is measured using an oscilloscope (TDS 224 Tektronix USA). The oscilloscope is interfaced to a computer using a GPIB card (National Instruments Inc.). On scanning, as the sample moves closer to the focus, there is a gradual increase in the light intensity and corresponding increase in the absorption; therefore, there is a decrease in the transmitted light that falls onto the detector. The experimental setup is first calibrated using Rh6G dye.<sup>26</sup>

### Computational details

DFT calculations have been carried out by using the *Gaussian 16, Revision B.01*.<sup>27</sup> All structural optimization was carried out by employing unrestricted B3LYP and CAM-B3LYP hybrid functional. The method used was Becke's three-parameter hybrid-exchange functional, the non-local correlation provided by the Lee, Yang, and Parr expression, and the Vosko, Wilk, and

Nuair 1980 correlation functional (III) for local correction.<sup>28</sup> The basis set was 6-31G\*\* for C, N, O, Cl, and H atoms and LANL2DZ for Ni and Cu atoms. Geometry optimizations were executed, and all the coordinates were taken from the molecular structures wherever possible. The optimized geometry was confirmed to be the potential energy minima by vibrational frequency calculations at the same level of theory as no imaginary frequencies were found. The orbital surfaces were visualized by *Chemcraft* software program. The HOMO and LUMO levels for all the molecules were also generated and prepared graphically with this software. The natural transition orbitals<sup>29</sup> were analysed based on the TD DFT method. The NCI<sup>30</sup> were constructed using Multiwfn software and visualized using VMD software.<sup>31</sup>

### Conflicts of Interest

The authors declare no competing financial interests.

### Acknowledgements

We thank the Science and Engineering Research Board (SERB), SERB-STAR, India, the Council of Scientific and Industrial Research (CSIR), New Delhi, STC (ISRO) India, and UGC New Delhi for financial support. The work in TMU was supported by a JST PRESTO (JPMJPR2103), and JSPS Grants-in-Aid (JP20H00406, JP21K18984, JP22K19937).

### Notes and references

- (a) R. Costil, M. Holzheimer, S. Crespi, N. A. Simeth, and B. L. Feringa, *Chem. Rev.*, 2021, **121**, 13213; (b) M. Baroncini, S. Silvi, and A. Credi, *Chem. Rev.*, 2020, **120**, 200; (c) V. García-López, D. Liu, and J. M. Tour, *Chem. Rev.*, 2020, **120**, 79; (d) F. Lancia, A. Ryabchun, and N. Katsonis, *Nat. Rev. Chem.*, 2019, **3**, 536.
- (a) L. Pfeifer, S. Crespi, P. van der Meulen, J. Kemmink, R. M. Scheek, M. F. Hilbers, W. J. Buma and B. L. Feringa, *Nat. Commun.*, 2022, **13**, 2124; (b) J. Volarić, W. Szymanski, N. A. Simeth, and B. L. Feringa, *Chem. Soc. Rev.*, 2021, **50**, 12377.
- (a) S. Crespi, N. A. Simeth, and B. König, *Nat. Rev. Chem.*, 2019, **3**, 133; (b) M. Hammerich, C. Schütt, C. Stähler, P. Lentjes, F. Röhricht, R. Höppner, and R. Herges, *J. Am. Chem. Soc.*, 2016, **138**, 13111; (c) H. M. D. Bandara, and S. C. Burdette, *Chem. Soc. Rev.*, 2012, **41**, 4422; (d) E. Merino, *Chem. Soc. Rev.*, 2011, **40**, 3835.
- (a) L. Kortekaas, and W. R. Browne, *Chem. Soc. Rev.*, 2019, **48**, 3406; (b) M. Irie, T. Fukaminato, K. Matsuda, and S. Kobatake, *Chem. Rev.*, 2014, **114**, 12174; (c) X. Su, and I. Arahamian, *Chem. Soc. Rev.*, 2014, **43**, 1963.
- (a) D. Villarón, and S. J. Wezenberg, *Angew. Chem., Int. Ed.*, 2020, **59**, 13192; (b) D. Roke, S. J. Wezenberg, and B. L. Feringa, *Proc. Natl Acad. Sci. USA.*, 2018, **115**, 9423; (c) A. Gerwien, P. Mayer, and H. Dube, *J. Am. Chem. Soc.*, 2018, **140**, 16442; (d) K. Mutoh, N. Miyashita, K. Arai, and J. Abe, *J. Am. Chem. Soc.*, 2019, **141**, 5650; (e) D.A. Leigh, *Angew. Chem. Int. Ed.*, 2016, **55**, 14506; (f) D. Bléger and S. Hecht, *Angew. Chem. Int. Ed.*, 2015, **54**, 11338;
- (a) S. Corra, M. Curcio, and A. Credi, *JACS Au.*, 2023, **3**, 1301; (b) B. Lukas, R. Pregizer and H. Dube, *J. Am. Chem. Soc.* 2023, **145**, 13081; (c) H. Wang, H. K. Bisoyi, X. Zhang, F. Hassan, and Q. Li, *Chem. Eur. J.*, 2022, **28**, e202103906. (d) X. Guo, J. Zhou, M. A. Siegler, A. E. Bragg, and H. E. Katz, *Angew. Chem. Int. Ed.*, 2015, **54**, 4782.
- (a) R. Toyoda, N. V. Hoang, K. Moghaddam, S. Crespi, D. R. S. Pooler, S. Faraji, M. S. Shenichnikov and B. L. Feringa, *Nat. Commun.*, 2022, **13**, 5765; (b) D. Taura, K. Shimizu, C. Yokota, R. Ikeda, Y. Suzuki, H. Iida, N. Ousaka and E. Yashima, *Chem. Commun.*, 2019, **55**, 12084; (c) (d) H.

- Yoon, J. M. Lim, H. Gee, C. Lee, Y. Jeong, D. Kim and W. Jang, *J. Am. Chem. Soc.*, 2014, **136**, 1672.
- 8 (a) A. Goswami, S. Saha, P. K. Biswas and M. Schmittle, *Chem. Rev.* 2020, **120**, 125; (b) A. Goswami and M. Schmittle, *Angew. Chem. Int. Ed.* 2020, **59**, 12362.
- 9 (a) I. Beletskaya, V. S. Tyurin, A. Y. Tsivadze, R. Guilard and C. Stern, *Chem. Rev.*, 2009, **109**, 1659; (b) P. D. Harvey, C. Stern, C. P. Gros and R. Guilard, *Coord. Chem. Rev.*, 2007, **251**, 401; (c) J. Rosenthal, J. Bachman, J. L. Dempsey, A. J. Esswein, T. G. Gray, J. M. Hodgkiss, D. R. Manke, T. D. Luckett, B. J. Pistorio, A. S. Veige and D. G. Nocera, *Coord. Chem. Rev.*, 2005, **249**, 1316.
- 10 (a) T. Tanaka and A. Osuka, *Chem. Soc. Rev.*, 2015, **44**, 943; (b) J. Yang, M.-C. Yoon, H. Yoo, P. Kim and D. Kim, *Chem. Soc. Rev.*, 2012, **41**, 4808; (c) J. S. Lindsey and D. F. Bocian, *Acc. Chem. Res.*, 2011, **44**, 638; (d) D. Gust, T. A. Moore and A. L. Moore, *Acc. Chem., Res.* 2009, **42**, 1890.
- 11 (a) D. Lai, F. S. T. Khan and S. P. Rath, *Adv. Inorg. Chem.* 2023, **81**, 95; (b) S. Sarkar, F. S. T. Khan, T. Guchhait and S. P. Rath, *Coord. Chem. Rev.* 2023, **479**, 215003; (c) D. Lai, F. S. T. Khan and S. P. Rath, *Dalton Trans.*, 2018, **47**, 14388; (d) T. Guchhait, S. Sasmal, F. S. T. Khan and S. P. Rath, *Coord. Chem. Rev.*, 2017, **337**, 112; (e) D. Sil, S. P. Rath, *Dalton Trans.* 2015, **44**, 16195.
- 12 (a) R. Wang, A. M. Brugh, J. Rawson, M. J. Therien and M. D. E. Forbes, *J. Am. Chem. Soc.*, 2017, **139**, 9759; (b) M. D. Peeks, C. E. Tait, P. Neuhaus, G. M. Fischer, M. Hoffmann, R. Haver, A. Cnossen, J. R. Harmer, C. R. Timmel and H. L. Anderson, *J. Am. Chem. Soc.*, 2017, **139**, 10461; (c) W. J. Cho, Y. Cho, S. K. Min, W. Y. Kim and K. S. Kim, *J. Am. Chem. Soc.*, 2011, **133**, 9364; (d) V. S. -Y. Lin, S. G. DiMagno and M. J. Therien, *Science* 1994, **264**, 1105
- 13 (a) Y. A. Pandit, S. J. Shah, M. Usman, S. Sarkar and S. P. Rath, *Inorg. Chem.*, 2022, **61**, 5270; (b) A. Kumar, S. Sanfui, G. Sciortino, J.-D. Maréchal, E. Garribba, and S. P. Rath, *Chem. Eur. J.*, 2020, **26**, 7869; (c) D. Sil, S. Dey, A. Kumar, S. Bhowmik and S. P. Rath, *Chem. Sci.*, 2016, **7**, 1212; (d) S. Dey, D. Sil and S. P. Rath, *Angew. Chem. Int. Ed.*, 2016, **55**, 996; (e) S. Dey, D. Sil, Y. A. Pandit and S. P. Rath, *Inorg. Chem.* 2016, **55**, 3229.
- 14 (a) S. J. Shah, Y. A. Pandit, E. Garribba, M. Ishida and S. P. Rath, *Chem. – Eur. J.*, 2023, **29**, e202301963; (b) A. K. Pandey, M. Usman and S. P. Rath, *Chem. Commun.*, 2019, **55**, 7926; (c) Y. A. Pandit, M. Usman, A. Sarkar, S. J. Shah and S. P. Rath, *Dalton Trans.* 2023, **52**, 877; (d) Y. A. Pandit, S. Sanfui and S. P. Rath, *Chem. Eur. J.* 2017, **23**, 13415.
- 15 (a) X. Zhang, S. Wang, Z. Fu, C. Wang, Z. Yang, Y. Gao, H. Liu, S. Zhang, C. Gu, and B. Yang, *Adv. Funct. Mater.*, 2023, **33**, 2301228; (b) G. Pan, Z. Wu, Z. Liu, B. Xu and W. Tian, *Angew. Chem. Int. Ed.*, 2023, **62**, e202303152.
- 16 The typical TPA values of porphyrin monomers are less than 100 GM; see (a) M. Yoon, S. B. Noh, A. Tsuda, Y. Nakamura, A. Osuka and D. Kim, *J. Am. Chem. Soc.*, 2007, **129**, 10080; (b) M. Drobizhev, Y. Stepanenko, Y. Dzenis, A. Karotki, A. Rebane, P. N. Taylor, and H. L. Anderson, *J. Am. Chem. Soc.*, 2004, **126**, 15352.
- 17 (a) K. Sugiura, G. Ponomarev, S. Okubo, A. Tajira and Y. Sakata, *Bull. Chem. Soc. Jpn.*, 1996, **70**, 1115; (b) L. Benthem, R. B. M. Koehorst and T. J. Schaafsma, *Magn. Reson. Chem.*, 1985, **23**, 732.
- 18 (a) D. E. Prokopchuk, E. S. Wiedner, E. D. Walter, C. V. Popescu, N. A. Piro, W. S. Kassel, R. M. Bullock and M. T. Mock, *J. Am. Chem. Soc.*, 2017, **139**, 9291; (b) K. A. Manbeck, N. C. Boaz, N. C. Bair, A. M. S. Sanders and A. L. Marsh, *J. Chem. Educ.*, 2011, **88**, 1444.
- 19 D. Geuenich, K. Hess, F. Köhler and R. Herges, *Chem. Rev.*, 2005, **105**, 3758.
- 20 (a) C. Dugave and L. Demange, *Chem. Rev.*, 2003, **103**, 2475; (b) D. H. Waldeck, *Chem. Rev.* 1991, **91**, 415.
- 21 (a) B. Zhang, Y. Feng and W. Feng, *Nano-Micro Lett.*, 2022, **14**, 138; (b) L. Zborovsky, A. Kostenko, D. Bravo-Zhivotovskii, and Y. Apeloig, *Angew. Chem. Int. Ed.*, 2019, **58**, 14524; (c) J. Saha, S. Banerjee, S. Malo, A. K. Das, and I. Das, *Chem. Eur. J.*, 2023, **29**, e 202302335; (d) A. Cnossen, J. C. M. Kistemaker, T. Kojima, and B. L. Feringa, *J. Org. Chem.*, 2014, **79**, 927.
- 22 SAINT+, 6.02 ed., Bruker AXS, Madison, WI, 1999.
- 23 G. M. Sheldrick, SADABS 2.0, 2000.
- 24 G. M. Sheldrick, SHELXL-2018: Program for Crystal Structure Refinement; University of Göttingen, Göttingen, Germany, 2018.
- 25 A. L. J. Spek, *Appl. Crystallogr.*, 2003, **36**, 7.
- 26 (a) P. Sengupta, J. Balaji, S. Banerjee, R. Philip, G. R. Kumar and S. Maiti, *J. Chem. Phys.*, 2000, **112**, 9201; (b) S. Das, A. Nag, D. Goswami and P. K. Bharadwaj, *J. Am. Chem. Soc.*, 2006, **128**, 402; (c) K. Pal, I. Samanta, R. K. Gupta, D. Goswami and A. L. Koner, *Chem. Comm.*, 2018, **54**, 10590; (d) R. Weber, K. Chok, S. Junek, C. Glaubitz and A. Heckel, *Chem. Eur. J.*, 2023, **29**, e202300149.
- 27 (a) M. J. T. Frisch, G. W. Trucks, H. B. Schlegel, G. E. Scuseria, M. A. C. Robb, J. R. Cheeseman, G. Scalmani, V. Barone, G. A. N. B. Mennucci, H. Petersson, M. Caricato, X. Li, H. Hratchian, A. F. Izmaylov, J. Bloino, G. Zheng, J. L. Sonnenberg, M. Hada, M. Ehara, K. Toyota, R. Fukuda, J. Hasegawa, M. Ishida, Y. K. T. Nakajima, O. Honda, H. Nakai, T. Vreven, J. A. Montgomery, J. E. O. Peralta, F. Oligaro, M. Bearpark, J. J. Heyd, E. Brothers, V. N. Kudin, K. K. N. R. Staroverov, J. Normand, K. Raghavachari, A. B. Rendell, S. S. Iyengar, J. Tomasi, M. Cossi, J. M. Rega, M. Millam, J. E. Knox, J. B. Cross, V. Bakken, C. J. Adamo, J. Gomperts, R. E. Stratmann, O. Yazyev, A. J. Austin, R. Cammi, J. W. Pomelli, J. W. Ochterski, R. L. Martin, K. Z. Morokuma, V. G. Zarkrzewski, G. A. Voth, P. Salvador, J. J. D. Dannenberg, S. Dapprich, A. D. Daniels, Ö. Farkas, J. B. Foresman, J. V. Ortiz, J. Cioslowski, D. J. Fox, Gaussian 16, Revision B.01, Gaussian, Inc., Wallingford, CT, 2016.
- 28 (a) S. Grimme, S. Ehrlich and L. Goerigk, *J. Comput. Chem.*, 2011, **32**, 1456; (b) S. Grimme, J. Antony, S. Ehrlich and H. Krieg, *J. Chem. Phys.*, 2010, **132**, 154104; (c) S. Grimme, *J. Comput. Chem.*, 2004, **25**, 1463; (d) S. Grimme, *J. Comput. Chem.*, 2006, **27**, 1787; (e) F. Weigend and R. Ahlrichs, *Phys. Chem. Chem. Phys.*, 2005, **7**, 3297.
- 29 Martin, R. L. *J. Chem. Phys.* 2003, **118**, 4775.
- 30 (a) R. A. Boto, F. Peccati, R. Laplaza, C. Quan, A. Carbone, J.-P. Piquemal, Y. Maday and J. Contreras-García, *J. Chem. Theory Comput.*, 2020, **16**, 4150; (b) J. Contreras-García, E. R. Johnson, S. Keinan, R. Chaudret, J.-P. Piquemal, D. N. Beratan and W. Yang, *J. Chem. Theory Comput.*, 2011, **7**, 625; (c) E. R. Johnson, S. Keinan, P. Mori-Sánchez, J. Contreras-García, A. J. Cohen and W. Yang, *J. Am. Chem. Soc.*, 2010, **132**, 6498.
- 31 W. Humphrey, A. Dalke, K. Schulten, *J. Molec. Graphics.*, 1996, **14**, 33.